Numerical study on nonlinear growth of $m/n=3/1$ double tearing mode in high Lundquist number regime

W. Guo[1], J. Ma[1], Q. Yu[2]

[1]Institute of Plasma Physics, Chinese Academy of sciences, Hefei 230031, People's Republic of China

[2]Max-Planck-Institut für Plasmaphysik, 85748 Garching, Germany

E-mail: wfguo@ipp.ac.cn and junma@ipp.ac.cn

Abstract

The nonlinear growth of the m/n=3/1 double tearing mode (DTM) is numerically investigated in cylinder geometry with non-monotonic radial profiles of the equilibrium safety factor, having two q=3 surfaces. The formation of plasmoids is found in high Lundquist number regime in such configurations for the first time. During the nonlinear growth of DTM, long and thin Sweet-Parker (SP) current sheets are formed near the original inner and outer rational surfaces and become tearing unstable for a large enough Lundquist number, leading to secondary and tertiary magnetic islands which accelerate the magnetic reconnection. The plasmoids also affect the magnetic topology at nonlinear mode saturation. The system can eventually saturate at a quasi-stationary state with small island pairs. The simulation results show that the Lundquist number and the distance between two rational surfaces have important effects on plasmoids formation.

1. Introduction

In tokamak experiments, non-monotonic radial profiles of the safety factor q with centrally reversed magnetic shear[1] can lead to the formation of the internal transport barrier and higher bootstrap current fraction than that in standard H-mode plasmas [2]-[4], being attractive for steady operation of a fusion reactor. However, as there are two rational surfaces with the same safety factor for such magnetic configurations, it is well known to be subject to resistive double tearing mode [5][6] (DTM), which can result in confinement degradation or even disruptions. Understanding of the

nonlinear evolution of DTM is therefore an important issue in fusion research. In addition to tokamak experiments, the DTM is also of great interest in the multiple current sheet system in space plasmas [7].

Many theoretical efforts have been devoted to investigate the DTM physics before, including the studies on both the linear and nonlinear growth of DTM. In the linear regime, it has been found [8][9] from the reduced MHD model that the resistivity dependence of the growth rate γ varies between $\gamma \sim \eta^{1/3}$ and $\gamma \sim \eta^{3/5}$, depending on the distance between the two rational surfaces. In nonlinear regime the DTM growth is also strongly affected by the separation of two rational surfaces. For a large enough separation, the magnetic islands grow and saturate more like two single tearing modes. When the two rational surfaces are closer, the coupling of inner and outer islands is enhanced. The inner magnetic islands expands toward the X points of outer ones, while the outer islands expands toward the X points of inner ones, leading to Sweet-Parker (SP) current sheets and flow-driven type magnetic reconnection process [9]-[13]. For rather closed rational surfaces, there could be broad linear spectra [14] with larger growth rate for the high mode numbers [15]. If the distance between the two resonant surfaces is too small, however, two resistive layers are merged into a single one, and the mode becomes stable [16]. Other effects on DTM, such as anomalous electron viscosity [17], Hall effect [18], shear flow [19][20], and guiding field [21][22], have also been studied

Most of the studies on DTM were carried out with relatively low Lundquist number (usually below 10^6). In existing tokamak experiments, however, the Lundquist number is much higher (10^7~10^9) [23]. In the high Lundquist number regime, recent results [24]-[30] indicate that the magnetic reconnection can be quite different from that in low Lundquist number regime. The SP current sheet may become tearing unstable and break up into plasmoids, leading to much faster reconnection than that predicted by the Sweet–Parker reconnection model. In slab geometry the SP current sheets become unstable for Lundquist number $S^* > 10^4$ (defined by characteristic length of SP current sheet) [31]-[37], and in toroidal geometry when poloidal magnetic field alone has been used for the definition of the local Lundquist number[38][39]. It is of great interest to learn if similar physics exists in the reversed magnetic shear configuration of tokamak plasmas, and how the nonlinear dynamics of DTM is affected by the Lundquist number and the q-profile.

For this purpose, a non-reduced conservative resistive MHD model [40][41] is extended to cylindrical geometry, which corresponds to the large aspect ratio approximation of tokamak plasmas, and a 5th order Weighted Essentially Non-Oscillatory (WENO) scheme is applied to build up a new numerical code. Using this new code, the nonlinear evolution of the m/n=3/1 DTM is numerically studied with the Lundquist number up to 10^7, where m and n are poloidal and toroidal mode numbers, respectively. This paper reports the major findings of our numerical calculations. Plasmoids formation is found for a sufficiently high Lundquist number, which accelerates the magnetic reconnection and affects the topology at nonlinear mode saturation. The distance between two $q = 3$ rational surfaces is also found to have an important effect on plasmoids formation.

In the next section the conservative resistive MHD model in cylindrical geometry and the numerical approaches for solving the nonlinear MHD equations are described. In Section 3, our numerical results are presented, followed by the discussion and summary in Section 4.

2. Physical Model

A straight cylindrical tokamak geometry with the plasma minor radius a and major radius R_0 is considered, in which the space coordinates are (r,θ,φ) with periodicity along the poloidal angle θ and toroidal angle φ. The non-reduced compressible MHD equations in conservative form of mass, momentum, energy and magnetic field are[41]

$$\partial_t \rho + \nabla\cdot(\rho\mathbf{V}) = 0 \quad (1)$$

$$\partial_t(\rho\mathbf{V}) + \nabla\cdot\left(\rho\mathbf{V}\mathbf{V} - \mathbf{B}\mathbf{B} + \left(p+\frac{1}{2}\mathbf{B}^2\right)\mathbf{I} - \nu\nabla\mathbf{V}\right) = 0 \quad (2)$$

$$\partial_t\left(\frac{p}{\Gamma-1}+\frac{1}{2}\left(\rho\mathbf{V}^2+\mathbf{B}^2\right)\right) + \nabla\cdot\left[\left(\frac{\Gamma p}{\Gamma-1}+\frac{1}{2}\rho\mathbf{V}^2+\mathbf{B}^2\right)\mathbf{V} - (\mathbf{B}\cdot\mathbf{V})\mathbf{B} - \nu\nabla\frac{\mathbf{V}^2}{2} + \eta\mathbf{J}\times\mathbf{B}\right] = \nabla\cdot\left(\eta\mathbf{J}_{eq}\times\mathbf{B}_{eq}\right) \quad (3)$$

$$\partial_t\mathbf{B} + \nabla\cdot(\mathbf{V}\mathbf{B} - \mathbf{B}\mathbf{V} - \eta\nabla\mathbf{B}) = \eta\nabla\mathbf{B}_{eq} \quad (4)$$

In addition, the divergence-free constraint of magnetic field, $\nabla\cdot\mathbf{B}=0$, is also applied. In above equations the subscript *eq* stands for equilibrium. $\Gamma = 5/3$. ρ, $\mathbf{V}$, p, $\mathbf{B}$, $\mathbf{J}$, ν, η are plasma density, velocity, pressure, magnetic field, current density, viscosity and resistivity, respectively. Following normalizations have been applied: $\rho/\rho_{00}\to\rho$, $p/(B_{00}^2/\mu_0)\to p$, $\mathbf{V}/V_A\to\mathbf{V}$, $\mathbf{B}/B_{00}\to\mathbf{B}$, $\mathbf{J}/(B_{00}/\mu_0 a)\to\mathbf{J}$, $\nu/(aV_A\rho_{00})\to\nu$, $\eta/(\mu_0 a^2/\tau_A)\to\eta$, $r/a\to r$, $R_0/a\to R_0$, $t/\tau_A\to t$, in which ρ_{00}, B_{00} are constant, $V_A=\sqrt{B_{00}^2/\mu_0\rho_{00}}$ is Alfvén speed, and $\tau_A = a/V_A$ is Alfvénic time. The Lundquist number is defined as $S = aV_A/\eta$. The general form of equation (1)-(4) can be written as

$$\partial_t U + \nabla\cdot\mathbf{F} = S_{eq} \tag{5}$$

where

$$U = \left(\rho, \rho V_x, \rho V_y, \rho V_z, \frac{p}{\Gamma - 1} + \frac{1}{2}\left(\rho \mathbf{V}^2 + \mathbf{B}^2\right), B_x, B_y, B_z \right)^T \tag{6}$$

is an array of mass, momentum, energy and magnetic field, $\mathbf{F}$ is the corresponding flux, and S_{eq} is source. In equation (6) the quantities are expressed in a Cartesian coordinate, being related to that in cylindrical geometry by the relations

$$\begin{cases} A_x = A_r \cos\theta - A_\theta \sin\theta \\ A_y = A_r \sin\theta + A_\theta \cos\theta \\ A_z = A_\varphi \end{cases} \tag{7}$$

The helical symmetry of scalar variables, $\rho(r,\theta,\varphi) = \rho(r,\zeta = \theta - (n/m)\varphi)$ is utilized. In the coordinates $(r,\ \zeta\ ,\varphi)$ equation (5) becomes

$$\partial_t\left(rU\right) + \partial_r\left(r\mathbf{e}_r\cdot\mathbf{F}\right) + \partial_\zeta\left[\left(\mathbf{e}_\theta - \frac{nr}{mR_0}\mathbf{e}_\varphi\right)\cdot\mathbf{F}\right] + \partial_\varphi\left(\frac{r}{R_0}\mathbf{e}_\varphi\cdot\mathbf{F}\right) = rS_{eq} \tag{8}$$

To solve equation (8) numerically, a 5th order accuracy of WENO method [42] based finite difference discretization and a flux-difference-splitting (FDS) approach [43] for generalized hyperbolic conservative system in smooth curvilinear grids are applied in the (r,ζ) computation domain. The divergence free condition on the magnetic field in computation is ensured by using the hyperbolic divergence cleaning (HDC) method proposed by Dedner[44]. In practical works we solve the perturbed form of (8). A new initial value code has been built up using above mentioned methods.

In order to check our initial value code, an eigenvalue code has also been built up. The comparison of the numerical results from the initial value code and eigenvalue code are given in the Appendix, indicating that they agree with each other.

The equilibrium condition in our work is basically $\nabla p = \mathbf{J}\times\mathbf{B}$**.** In addition the source terms are added in equations (3) and (4) to satisfy energy and magnetic field balance in the absence of perturbations. A non-monotonic radial profile for the original equilibrium safety factor is assumed for our calculations,

$$q(r) = q_c \left\{ 1 + \left(\frac{r}{r_0} \right)^{2\lambda} \right\}^{1/\lambda} \left[1 + c \exp\left\{ -\left(\frac{r - r_\delta}{\delta} \right)^2 \right\} \right] \tag{9}$$

with $\lambda = 1$, $r_0 = 0.412$, $\delta = 0.273$, $r_\delta = 0$, and $c = 3$. The value of q_c is varied to have different radial positions of $q = 3$ resonant surfaces at r = r_1 and r_2, as shown in figure 1, where $\Delta r = (r_2 - r_1)$ is the distance between the two resonant surfaces.

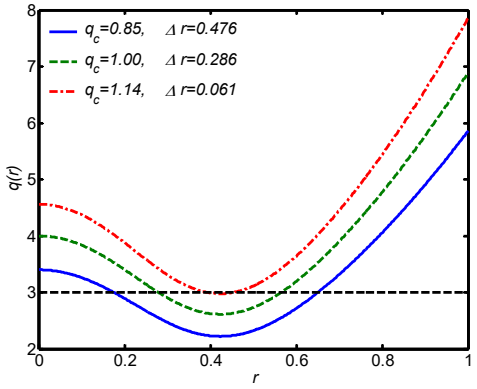

Figure 1 Radial profiles of the safety factor $q(r)$ with different separations between two rational surfaces.

Other input parameters used in our simulations are $R_0 = 4a$ and $\nu = 1 \times 10^{-10}$. The plasma resistivity η is assumed to be a constant in space. Different Lundquist number *S* is used in calculations by varying the η value. The radial computation domain is from 0 to a. We have used different number of grids to test the numerical convergence. The radial grid number varies from 1000 up to 2400 and poloidal grid number from 192 to 768. It was found that comparing the results from 1500×384 grids to that from more grids, the difference in the linear growth rate is less than 1%, and the nonlinear results are quite similar. The time step is determined though the CFL condition with a fixed CFL number 0.8. In addition to the m/n=3/1 component, high harmonics of m/n=3/1 component, such as m/n=6/2, 9/3, … as well as the 0/0 component are also taken into account in our calculations.

3. Numerical Results

We first look into the nonlinear growth of DTM in low Lundquist number regime ($S < 10^6$). One important feature of the nonlinear evolution of DTM is the formation of Sweet-Parker type current

sheets (with a smaller Δr) or even sharp current points (with a larger Δr) as reported in previous works [10]. These results are reproduced using our initial value code. One example is displayed in figure 2 with $S = 2 \times 10^5$ and Δr=0.182. Figures 2 (a) to (d) show the magnetic surfaces at different times. It is seen that during the DTM growth, the inner magnetic islands grows outwards toward the X points of outer ones, while the outer islands grows inwards toward the X points of inner ones, indicating the strong coupling between the inner and outer magnetic islands and a flow-driven type magnetic reconnection process.

Figure 2 (e) and (f) shows the corresponding radial profiles of the safety factor and plasma current density at the beginning (t=0) and at nonlinear mode saturation (t=1370). The q-profile flattens to about q=3 in the region between the original two q=3 surfaces, as also seen from existing publications [6][9][13]. The current density profile significantly changes around two q=3 surfaces and in the region between them, while the total current remains the same as the initial one due to the source electric field in Ohm's law. In this example intensive SP currents sheets near X points are observed, while current points have been found in other examples, e.g. $\Delta r = 0.286$. These results are in agreement with previous findings [9]-[13], and no plasmoids are found.

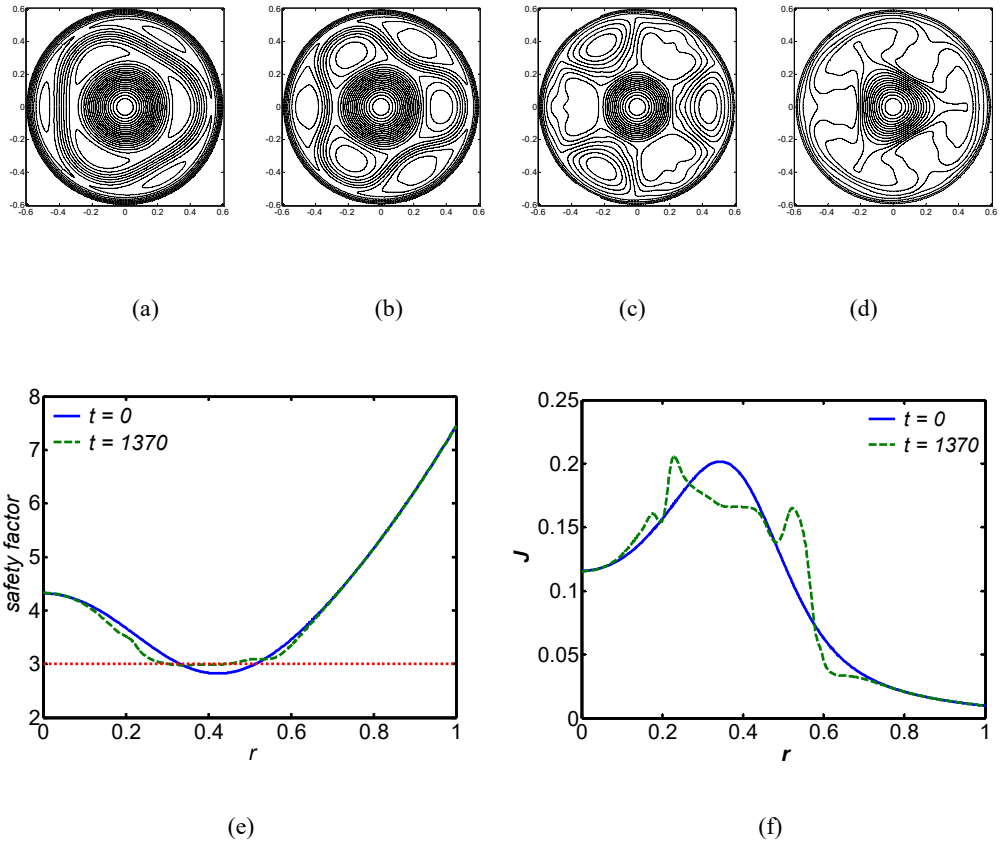

Figure 2 Nonlinear evolution of DTM with $S = 2 \times 10^5$ and $\Delta r = 0.182$. The poloidal magnetic surfaces at (a) t = 700, (b) t = 900, (c) t = 1100, and (d) t = 1370. The safety factor and current density profiles at t = 0 and t =

1370 are plotted in (e) and (f).

For higher Lundquist numbers, the nonlinear evolution of DTM has a big difference from that for lower ones, and plasmoids are observed frequently. The critical value of Lundquist number [34][35] for plasmoid instability defined by $S^* = lV_A/\eta = S \cdot l/a$, where l is half-length of SP current sheet, is also given below. An example with $S = 5 \times 10^6$ and $\Delta r = 0.182$ is shown in Figure 3. The contour lines show the poloidal magnetic surfaces, and the color maps indicate the toroidal current density J_φ at different time. During the nonlinear growth of DTM, long and thin SP current sheets are formed near the X points of the inner and outer islands at $r = 0.563$ and $r = 0.270$, respectively, as shown in the figure (a). The outer current sheets become unstable first, and m/n=3/1 secondary islands arise from the central part of the outer current sheets at the poloidal angle 0, $2\pi/3$ and $4\pi/3$, separating the outer SP current sheets into equal ribbons, as displayed in figure (b). The maximum length-to-thickness aspect ratio of outer current sheet reaches $\alpha_{\text{out}} \approx 45.1$ (at $\text{t} = 3020$) with $S^*_{out} \approx 9.7 \times 10^5$ before breaking up, meanwhile the aspect ratio of the inner current sheets reaches $\alpha_{in} \approx 28.9$. As the outer secondary islands grow, the inner current sheets develop with increasing aspect ratio, and the inner secondary islands appear until α_{in} reaches 39.3 with $S^*_{in} \approx 7.1 \times 10^5$, as seen from figure 3 (c). Afterwards the outer secondary islands expand slowly inward and the inner secondary islands expand outward, thus the outer and inner main islands are squeezed to form new current sheets and become unstable, which give rise to tertiary islands, as shown in (d) and (e). When the tertiary islands grows, the secondary islands start to shrink until they are about equal in size, forming quasi-stationary m/n=3/1 island pairs that only decay at the current diffusion time scale, as shown in (e). An interesting fact is that the outer plasmoids can reach larger size than the inner ones. This is also true in the final quasi-stationary state. The time evolution of kinetic energy and magnetic energy is shown in figure (f), covering both the linear (t<1100) and nonlinear stage, and the time spots of outer and inner plasmoids formation are pointed out by arrows.

This novel quasi-stationary state with multiple island pairs is formed mainly due to two reasons. The first one is the formation of tertiary islands as a consequence of secondary islands evolution. Since the secondary and tertiary islands have inverse magnetic flux, they cannot merge, so that the island pairs are maintained. Without this tertiary island the secondary island will keep reconnecting until it disappears, leading to a conventional quasi-stationary state as reported in previous works. The second reason is the poloidal symmetry of magnetic flux in each m/n=3/1 sector is exactly preserved in our simulations. A very slight poloidal asymmetry induced either by initial setup or during simulation by numerical error will not lead to visible effect before the generation of tertiary islands. When a tertiary island grows, however, the poloidal asymmetry leads to poloidal shift of the tertiary island, and then the secondary and tertiary islands will escape from each other and quickly shrink, and the system decays to a conventional state.

A sufficiently high Lundquist number S is always found to be required for the generation of plasmoids in our calculations, since the SP current sheets become thinner with decreasing resistivity. In general a current sheet becomes unstable only when a sufficiently large aspect ratio is reached. In above example, both inner and outer plasmoids are formed. In other cases inner plasmoids are not generated even if there are outer ones. This is due to the radial asymmetry of inner and outer current sheets, to be addressed in the following.

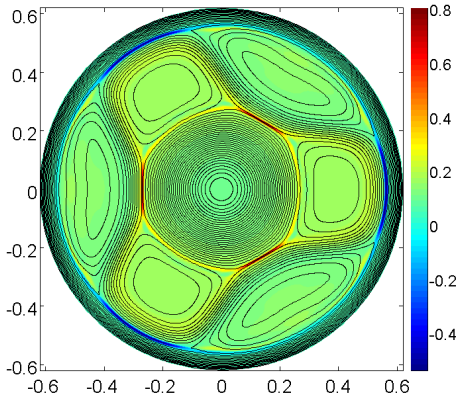

(a)

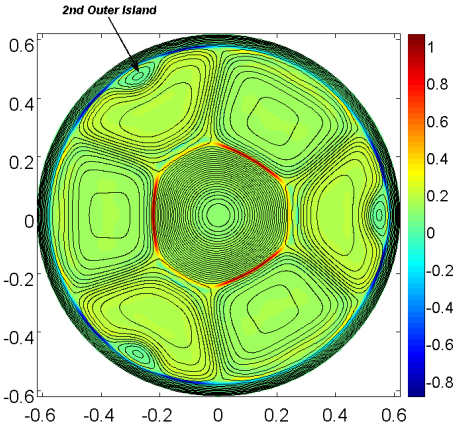

(b)

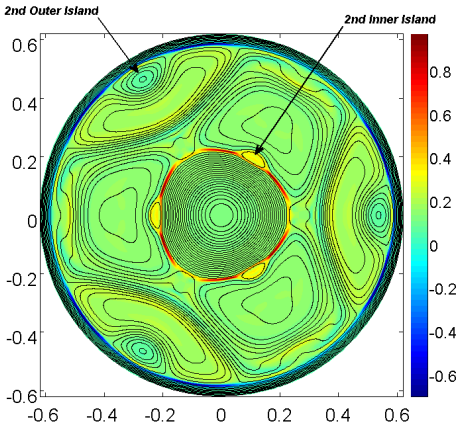

(c)

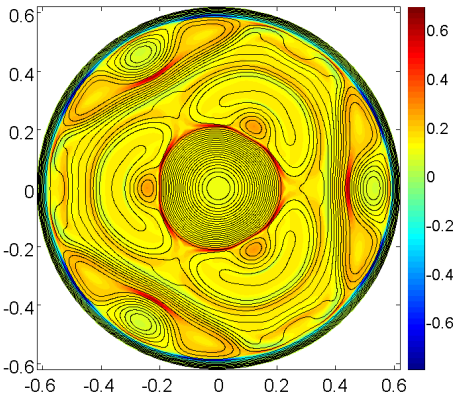

(d)

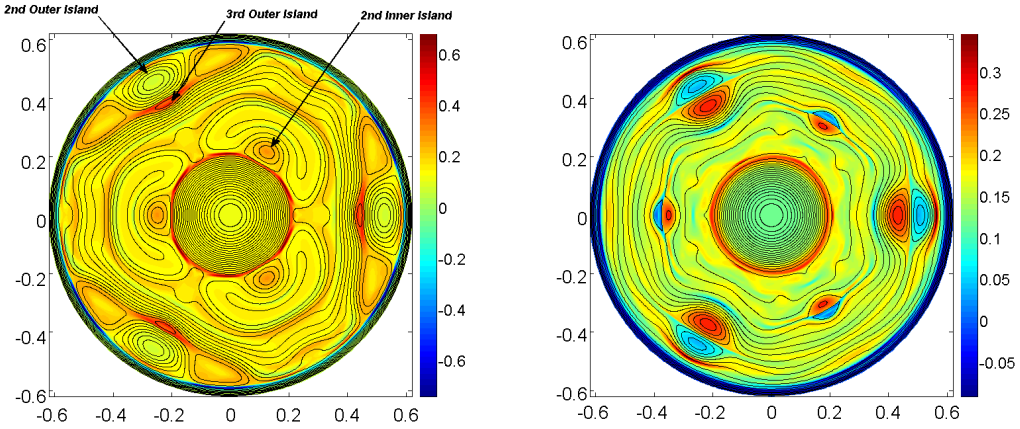

(e) (f)

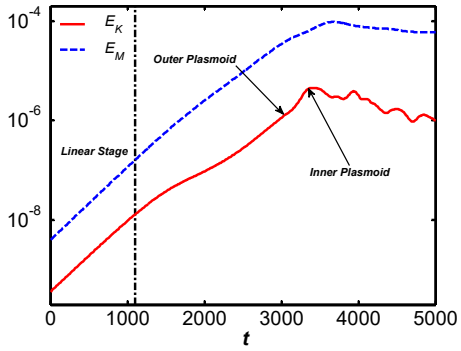

(g)

Figure 3 Plasmoids formation and evolution in high Lundquist number regime with $S = 5 \times 10^6$ and $\Delta r = 0.182$. The poloidal magnetic surface (contour lines) and the toroidal current density J_φ (color maps) are displayed at different time, (a) t=3000, (b) t=3330, (c) t=3500, (d) t=3680, (e) t=3750, and (f) t=4500. The time evolution of kinetic energy (E_K) and magnetic energy (E_M) is plotted in (g).

In addition to the Lundquist number, the distance between two resonant surfaces also significantly affects the results. Plasmoids formation has been observed only for an intermediate range of Δr. For a too small Δr, e.g. $\Delta r = 0.114$, the minimum value of the safety factor, $q_{min} = 2.93$, is close to $q = 3$ and the fraction of the $q < 3$ part is too small, so there is no enough free energy to drive the flow-driven reconnecting SP current sheets. For a too large Δr, e.g. Δr =0.310, the SP current sheets formed near X points are too short, and the aspect ratio is not high enough similar to that of a single tearing mode.

Furthermore, the effect of Δr upon the inner and outer plasmoids is different. The generation of outer plasmoids is robust for $S \geq 10^6$ and $0.151 \leq \Delta r \leq 0.286$. However, the generation of inner

plasmoids requires higher Lundquist number and a narrower range of Δr. For $S = 2 \times 10^6$, inner plasmoids are found for relatively small Δr, e.g. $\Delta r = 0.151$ and $\Delta r = 0.182$. Locating at a smaller minor radius, the inner SP current sheets are usually shorter than outer ones. When Δr is further increased, the inner rational surface is located closer to r=0, thus the length of inner SP current sheets are shorter, resulting in a lower aspect ratio of the current sheet. With $\Delta r = 0.224$, inner secondary island is observed for $S \geq 5 \times 10^6$. For an even larger value of Δr, $\Delta r = 0.249$, the poloidal elongation of inner SP current sheets is severely restricted, as shown in figure 4 for $S = 5 \times 10^6$. The inner SP current sheets form near $r = 0.17$ as seen from figure (a), and later they move inward during nonlinear mode growth as shown in figure (b). The maximum aspect ratio during DTM evolution is $\alpha_{in} \approx 26$. No inner plasmoids form in this case, while the outer plasmoids are generated and a quasi-stationary state with outer island pairs is reached. For such a value of Δr, inner plasmoids are absent even for $S = 10^7$. This indicates that the minor radius of the inner resonant surface, which changes during the nonlinear mode growth, also affects the local plasmoids formation.

Similarly, the difference in the birth time of outer and inner secondary islands is also affected by Δr. The inner secondary islands always form later than outer ones, with a time delay Δt_{io}. When Δr is increased, Δt_{io} becomes larger. For example, in the cases with $S = 5 \times 10^6$, $\Delta t_{io} \cong 70$ for $\Delta r = 0.151$, $\Delta t_{io} \cong 330$ for $\Delta r = 0.182$ and $\Delta t_{io} \cong 460$ for $\Delta r = 0.224$.

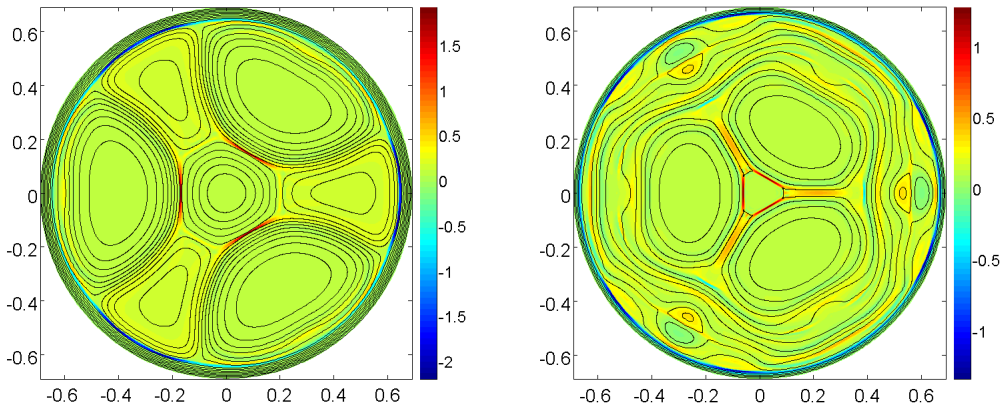

(a) (b)

Figure 4 Poloidal magnetic surfaces at (a) t=7400 and (b) t=7800 for $\Delta r = 0.249$ and $S = 5 \times 10^6$. The inner SP current sheets move inward and become shorter during mode growth.

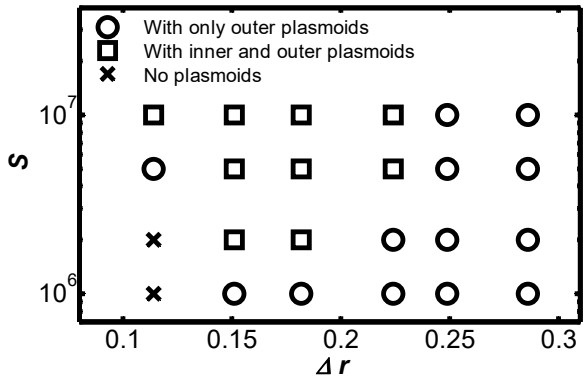

Figure 5 Plasmoids generation during nonlinear growth of DTM shown in the $S - \Delta r$ plane. Three different types of results are marked: With only outer plasmoids (circles), with both inner and outer plasmoids (squares), and no plasmoids (crosses).

The plasmoids generation mentioned above is summarized in a $S - \Delta r$ plane in Figure 5. A high enough Lundquist number, $S = 10^6$, is required for outer plasmoids generation and $S = 2 \times 10^6$ for inner ones. The corresponding critical values of S^* $(= S \cdot l/a)$ are $S^* \approx 1.9 \times 10^5$ and $S^* \approx 2.8 \times 10^5$ for the outer and inner plasmoids generation. Both values are higher than the critical value $S^* \sim 10^4$ in slab geometry. The amplitude of poloidal field around the current sheet is about 4%~5% of the toroidal filed. Using the poloidal field in the definition of the minimum local Lundquist number lead to the value $4 \times 10^4 \sim 5 \times 10^4$ for plasmoids generation, and the value is about 10^4 when further taking into account the length of current sheet.

To study the reconnection rate related to plasmoids in high Lundquist number regime, the outer secondary island width, *w*, at different time is measured, and its growth speed $\frac{dw}{dt}$ is calculated when *w* grows from 0.02 a to 0.1 a. The reconnection rate related to plasmoids is defined as

$$Rate = a\left(\frac{dw}{dt}\right)^{-1} \tag{10}$$

and displayed by the curve with crosses in figure 6 for different Lundquist numbers. The reconnection rates predicted from other models are also plotted for comparison. The dot dash line and dashed line show the classical tearing mode scaling ($\sim S^{-3/5}$) and Sweet-Parker reconnection scaling ($\sim S^{-1/2}$), respectively, with the assumption that they have the same value as the numerical results for $S = 10^6$, in order to illustrate the different slope of the curves. It is seen that with increasing Lundquist number, the reconnection rate is larger than that given by the tearing mode and Sweet-Parker scaling, indicating that the formation of plasmoids accelerates the reconnection.

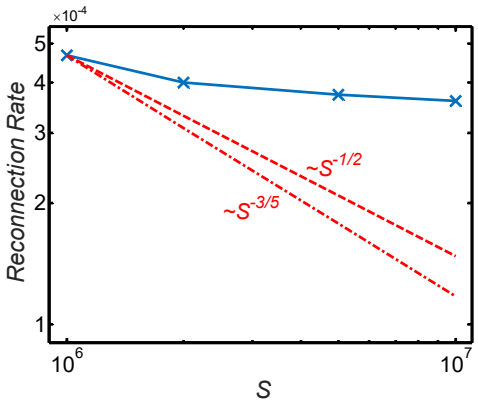

Figure 6 Reconnection rate versus S. The curve with crosses represents the reconnection rate of m/n=3/1 outer secondary islands obtained numerically. The dot dash line and dashed line show the classical tearing mode scaling ($\sim S^{-3/5}$) and Sweet-Parker reconnection scaling ($\sim S^{-1/2}$), respectively, with the assumption that they have the same value as the numerical results for $S = 10^6$.

4. Discussion and Summary

In recent simulations of the resistive internal kink mode instability of tokamak plasmas, plasmoids were found to appear during sawtooth crashes for $S > 10^6$, as seen from figure 4 of reference [45]. This S value is close to that of our results found in the nonlinear growth of DTM. Differing from the slow growth of a single resistive tearing mode, both the internal kink mode and the DTM have a common feature, the accelerated mode growth and resulting thin current sheet in the nonlinear phase. These indicate that plasmoids formation is a fundamental phenomenon for the fast growing nonlinear MHD instabilities in tokamak plasmas, in which the S value is usually larger than 10^7 except in the region being very close to the plasma edge. High Lundquist number S required for the generation of plasmoids is as expected, since a large plasma resistivity causes a fast resistive diffusion of a current sheet, increasing its width and decreasing its aspect ratio, and the critical aspect ratio for plasmoids formation cannot be reached.

Previous numerical works [32]-[37] have revealed that in slab geometry, when the Lundquist number is high enough ($S^*\sim 10^4$), the length-to-thickness aspect ratio $\alpha = L/\delta_{SP}$ of the SP current sheets rises to the level 10^2. Then the SP current sheets break up, leading to plasmoids. This threshold value of S for plasmoids formation in slab geometry is much lower than that in cylinder geometry. If we use poloidal magnetic field and length of SP current sheet in the definition, the critical Lundquist number is about 10^4 similar to the previous definitions in tokamaks[38][39]. Another difference between the cylinder and slab geometry is the asymmetry of the plasmoids formation at two resonant

surfaces in cylinder geometry. The inner SP current sheets are usually shorter than outer ones when the plasma resistivity is assumed to be a constant in space. Considering that the electron temperature is higher in the central region of tokamak plasmas, the plasma resistivity is smaller at the inner resonant surface. This suggests that inner plasmoids can be generated more easily in experiments than the results shown in this paper, depending on the radial profiles of the safety factor and plasma resistivity.

The distance between two resonant surfaces (Δr) affects plasmoids formation as shown in figure 5. It is worth to point out that the amplitude of equilibrium magnetic shear on both q = 3 rational surfaces reduces monotonically with reducing Δr, so that the effect of Δr upon plasmoids formation and evolution also includes the contribution of the change in magnetic shear. A further investigation of shear effect alone is still required.

Our study is limited to the m/n=3/1 DTM with two q = 3 rational surfaces in a cylindrical geometry. For different mode numbers and q-profiles, the nonlinear dynamics might be different, since the mode growth rate and the poloidal elongation of current sheets are different. The m/n=3/1 DTM in cylinder geometry has helical symmetry, and only components with the same helicity, such as the m/n=6/2, 9/3, ... are coupled together (in addition to the 0/0 component) during the nonlinear mode growth. The growth of these high harmonics due to nonlinear mode coupling leads to the plasmoids. In a realistic toroidal geometry, mode coupling between modes with different helicity is inevitable, which might lead to different dynamics of plasmoids.

In summary, a new initial value code has been developed in cylinder geometry based on the conservative perturbed resistive MHD model and a conservative finite difference method of 5^{th} order of accuracy. Using this new code, the nonlinear evolution of m/n=3/1 DTM is studied numerically in the configuration with centrally reversed magnetic shear, and plasmoids formations are observed in such a configuration for the first time. The nonlinear dynamics in the low and high Lundquist number regimes are found to be quite different. For $S \geq 10^6$, the aspect ratio of SP current sheets reaches the critical value, and plasmoids near outer and inner rational surfaces are formed with appropriate distance between two resonant surfaces. A quasi-stationary state with m/n=3/1 island pairs are reached. The magnetic reconnections related with plasmoids formation are accelerated in high Lundquist number regime.

Acknowledgments

The numerical calculations are performed on the ShenMa High Performance Computing Cluster at the Institute of Plasma Physics, Chinese Academy of Sciences. This work is supported by the

National Key R&D Program of China under Grant No. 2017YFE0300402 and the National Natural Science Foundation of China under Grant No. 11475219 and 11775268. The work is also supported by the Major / Innovative Program of Development Foundation of Hefei Center for Physical Science and Technology under Grant No. 2018CXFX009.

References

[1] Levinton F. M. *et al.* 1995 *Phys. Rev. Lett*. **75** 4417

[2] Fujita T. *et al.* 1997 *Phys. Rev. Lett.* **78** 2377

[3] Eriksson L.-G. *et al.* 2002 *Phys. Rev. Lett.* **88** 145001

[4] Joffrin E. *et al.* 2003 *Nucl. Fusion* **43** 1167

[5] Chang Z. *et al.* 1996 *Phys. Rev. Lett.* **77** 3553

[6] Gütner S. *et al.* 2000 *Nucl. Fusion* **40** 1541

[7] Wang Z.X. et al. 2007 *Phys. Rev. Lett.* **99** 185004

[8] Pritchett P.L. and Lee Y.C. 1980 *Phys. Fluids* **23** 1368

[9] Ishii Y. *et al.* 2000 *Phys. Plasmas* **7** 4477

[10] Ishii Y. *et al.* 2002 *Phys. Rev. Lett*. **89** 205002

[11] Ishii Y. *et al.* 2003 *Nucl. Fusion* **43** 539

[12] Ishii Y. *et al.* 2003 *Phys. Plasmas* **10** 3512

[13] Sato M. *et al.* 2001 *J. Phys. Soc. JPN.* **70** 2578

[14] Bierwage A. *et al.* 2000 *Phys. Plasmas* **12** 082504

[15] Bierwage A. *et al.* 2003 *Phys. Plasmas* **14** 022107

[16] Yu Q. and Gütner S. 1999 *Nucl. Fusion* **39** 487

[17] Dong J.Q., Mahajan S.M. and Horton W. 2003 *Phys. Plasmas* **10** 3151

[18] Zhang C.L. and Ma Z.W. 2009 *Phys. Plasmas* **16** 122113

[19] Wang X.Q., Xu W.B. and Wang Z.X. 2011 *Plasma Phys. Controlled Fusion* **53** 62003

[20] Mao A., Li J.Q., Kishimoto Y. and Liu J.Y. 2013 *Phys. Plasmas* **20** 022114

[21] Pritchett P.L. 2005 *Phys. Plasmas* **12** 062301

[22] Huba J.D. 2005 *Phys. Plasmas* **12** 012322

[23] Gütner S., Yu Q., Lackner K., Bhattacharjee A. and Huang Y.-M. 2015 *Plasma Phys. Control. Fusion* **57** 014017

[24] Lee L.C. and Fu Z.F. 1986 *J. Geophys. Res.* **91** 6807

[25] Biskamp D. 1986 *Phys. Fluids* **29** 1520

[26] Loureiro N.F. *et al.* 2016 *Plasma Phys. Control. Fusion* **58** 014021

[27] Loureiro N.F. *et al.* 2007 *Phys. Plasmas* **14** 100703

[28] Loureiro N.F. *et al.* 2013 *Phys. Rev. E* **87** 013102

[29] Samtaney R. *et al.* 2009 *Phys. Rev. Lett.* **103** 105004

[30] Ni L. *et al.* 2010 *Phys. Plasmas* **17** 052109

[31] Zhang C.L. and Ma Z.W. 2011 *Phys. Plasmas* **18** 052303

[32] Nemati M.J., Wang Z.X. and Wei L. 2016 *Astrophys. J.* **821** 128

[33] Nemati M.J., Wang Z.X. and Wei L. 2017 *Astrophys. J.* **835** 191

[34] Tenerani A., Velli M., Rappazzo A. F. and Pucci F. 2015 *Astrophys. J. Lett.* **813** L32

[35] Baty H. 2017 *Astrophys. J.* **837** 74

[36] Guo W., Ma J. and Yu Z. 2017 *Phys. Plasmas* **24** 032115

[37] Ma J., Guo W., Yu Z. and Yu Q. 2017 *Nucl. Fusion* **57** 126004

[38] Ebrahimi F. and Raman R. 2015 *Phys. Rev. Lett*. **114** 205003

[39] Ebrahimi F. 2016 *Phys. Plasmas* **23** 120705

[40] Ma J., Guo W. and Yu Z. 2017 *Commun. Comput. Phys.* **21** 1429

[41] Goedbloed J.P. and Poedts S. 2004 *Principles of Magnetohydrodynamics with Applications to Laboratory and Astrophysical Plasmas* (Cambridge: Cambridge University Press) (https://doi.org/10.1017/CBO9780511616945)

[42] Shu C.W. 1997 *ICASE Report No. 97-65 NASA/CR-97-206253, ICASE Report No. 97-65* NASA Langley Research Center (https://ntrs.nasa.gov/archive/nasa/casi.ntrs.nasa.gov/19980007543.pdf)

[43] Jiang Y., Shu C. W., Zhang M. P. 2014 *Methods Appl. Anal.* **21** 1

[44] Dedner A., Kemm F., Kröner D., Munz C.-D., Schnitzer T. and Wesenberg M. 2002 *J. Compt. Phys.* **175** 645

[45] Yu Q., Gütner S. and Lackner K. 2014 *Nucl. Fusion* **54** 072005

Appendix Benchmark between the initial value and eigenvalue codes

For linear analysis, the eigenvalue method is also used. Linearizing equations (1)-(4) and applying Fourier transform upon linear terms like $\tilde{\rho} = \rho_{m,n}(r)e^{\gamma t - i(m\theta - n\varphi)}$, where γ is linear growth rate, one has $\partial_t \to \gamma$, $\partial_\theta \to -im$ and $\partial_\varphi \to in$. In radial direction a 4th order finite difference discretization of the operators ∂_r is applied, forming the following eigenvalue problem

$$AX_{m,n} = \gamma X_{m,n} \tag{A1}$$

in which A is a matrix containing given parameters and discretized radial differential operators, and $X_{m,n} = (\rho, V_r, V_\theta, V_\varphi, p, B_r, B_\theta, B_\varphi)^T_{m,n}$ is a vector of variables. Solving equation (A1) the linear growth rate and corresponding radial eigenmode structures are obtained. An eigenvalue code has been built up to benchmark the result of initial value code in the linear regime. For the initial value code, a sufficiently small initial perturbation is taken in order to obtain the linear results [40].

The results obtained from both codes are presented in Figure A1, showing the linear growth rates as a function of Lundquist number (Figure A1(a)) and Δr (Figure A1(b)). It is seen that the results from these two approaches are very close. The eigenmode structures of V_r and B_r from both codes are also quite close. An example with $S = 5 \times 10^6$ and $\Delta r = 0.286$ is displayed in Figure A1(c) and (d).

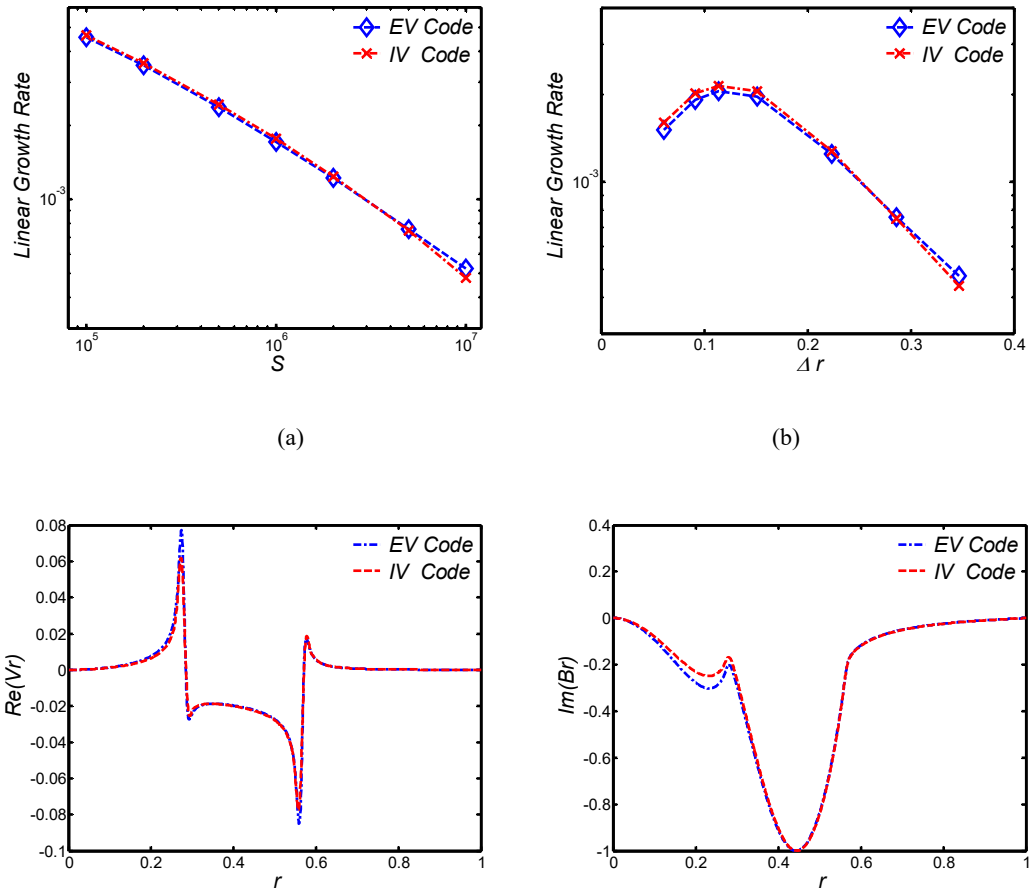

Figure A1 Comparisons of linear results from eigenvalue code (EV code) and initial value code (IV code). (a) Linear growth rate versus S with $\Delta r = 0.286$. (b) Linear growth rates versus Δr with $S = 5 \times 10^6$. (c) Radial profiles of radial plasma velocity V_r and (d) Radial profiles of radial magnetic field B_r, with $S = 5 \times 10^6$ and $\Delta r = 0.286$.